ZIRCON U-PB RESULTS FROM THE EASTERN MORAN AREA, TANANA B-6 AND MELOZITNA B-1 QUADRANGLES, ALASKA

Lawrence K. Freeman, Paul B. O'Sullivan, and Alec D. Wildland

Raw Data File 2023-15

2023
STATE OF ALASKA
DEPARTMENT OF NATURAL RESOURCES
DIVISION OF GEOLOGICAL & GEOPHYSICAL SURVEYS

STATE OF ALASKA
Mike Dunleavy, Governor

DEPARTMENT OF NATURAL RESOURCES
John Boyle, Commissioner

DIVISION OF GEOLOGICAL & GEOPHYSICAL SURVEYS
David L. LePain, State Geologist & Director

Publications produced by the Division of Geological & Geophysical Surveys are available to download from the DGGS website (dggs.alaska.gov). Publications on hard-copy or digital media can be examined or purchased in the Fairbanks office:

Alaska Division of Geological & Geophysical Surveys (DGGS)
3354 College Road | Fairbanks, Alaska 99709-3707
Phone: 907.451.5010 | Fax 907.451.5050
dggspubs@alaska.gov | dggs.alaska.gov

DGGS publications are also available at:

Alaska State Library, Historical
Collections & Talking Book Center
395 Whittier Street
Juneau, Alaska 99801

Alaska Resource Library and
Information Services (ARLIS)
3150 C Street, Suite 100
Anchorage, Alaska 99503

Suggested citation:
Freeman, L.K., O'Sullivan, P.B., and Wildland, A.D., 2023, Zircon U-Pb results from the eastern Moran area, Tanana B-6 and Melozitna B-1 quadrangles, Alaska: Alaska Division of Geological & Geophysical Surveys Raw Data File 2023-15, 18 p. https://doi.org/10.14509/31016

ZIRCON U-PB RESULTS FROM THE EASTERN MORAN AREA, TANANA B-6 AND MELOZITNA B-1 QUADRANGLES, ALASKA

Lawrence K. Freeman[1], Paul B. O'Sullivan[2], and Alec D. Wildland[1]

INTRODUCTION

In 2011, geologists from the Alaska Division of Geological & Geophysical Surveys (DGGS) conducted field studies in the eastern Moran area as part of an integrated geological, geophysical, and geochemical mineral inventory study in the eastern Kokrines Hills near Moran Dome in the Tanana B-6 and Melozitna B-1 quadrangles (fig. 1). This work was part of the Alaska Airborne Geophysical/Geological Mineral Inventory (AGGMI) program and included geologic mapping under the U.S. Geological Survey (USGS) STATEMAP program. Previous geologic work in the area is at a reconnaissance scale (Chapman and others, 1982), although two localities in the study area have undergone detailed mineral-resource evaluations (Tozimoran Creek placer [Thomas and Wright, 1948; Chapman and others, 1963; Barker and Warner, 1985] and Monday Creek [International Tower Hill Mines, Ltd., 2006, 2007]). A bedrock geologic map by DGGS of the eastern Moran area (Freeman and others, 2022) includes data published herein.

$^{40}Ar/^{39}Ar$ geochronology from the Moran area (Benowitz and others, 2019) updates the limited geochronology of the region. Orthogneiss in the Ruby terrane in the Kokrines Hills has a zircon U-Pb age, indicating crystallization at 380 to 390 million years (Ma) (Roeske and others, 2006). Gabbro from the Tozitna terrane (Rampart Group) has a hornblende K/Ar age of 210 ± 6 Ma (Patton and others, 1977) and $^{40}Ar/^{39}Ar$ age of 231.5 ± 1.9 Ma (Benowitz and others, 2019). K/Ar ages of Ruby terrane rocks in the Kokrines Hills (Melozitna Quadrangle) indicate peak blueschist-facies metamorphism occurred prior to ~144 Ma with a greenschist-facies overprint at ~133 Ma (Roeske and others, 1995). In the Moran area, $^{40}Ar/^{39}Ar$ ages indicate the minimum age of prograde metamorphism of Ruby terrane rocks ranges from 148.5 ± 1.7 to 140.4 ± 1.7 Ma and retrograde greenschist metamorphism is 122.6 ± 2.3 Ma (Benowitz and others, 2019). The retrograde metamorphism in the Moran area is roughly coeval with the age of fabric development parallel to the Kaltag fault (128.3 ± 1.7 Ma) and Tozitna thrust/detachment fault (123.2 ± 1.5 Ma) in the same area (Benowitz and others, 2019). A subsequent localized cooling age of ~109 Ma was measured from an amphibolite body in the western Kokrines Hills (Roeske and others, 1995). Ruby terrane amphibolite-grade schist and gneiss (Puchner and others, 1998) have a $^{40}Ar/^{39}Ar$ biotite age of 64.3 ± 0.6 Ma and $^{40}Ar/^{39}Ar$ muscovite ages of 71.3 ± 0.8 Ma and 76.9 ± 0.7 Ma (Benowitz and others, 2019). The Melozitna pluton has biotite K/Ar ages of 111 ± 3 Ma (Patton and others, 1977) and $^{40}Ar/^{39}Ar$ age of 116.5 ± 1.3 (Benowitz and others, 2019). Dikes within the Melozitna pluton have $^{40}Ar/^{39}Ar$ biotite ages of 105.7 ± 1.1 and 110.1 ± 1.3 Ma and a $^{40}Ar/^{39}Ar$ whole-rock age of 102.8 ± 1.2 Ma (Benowitz and others, 2019). Mineralized galena veins in the Tozimoran drainage have a white mica age of 119.0 ± 1.3 Ma. An auriferous vein from the Monday Creek area has an interpreted age of 66.5 ± 2.6 (Benowitz and others, 2019).

[1] 3354 College Road, Fairbanks, AK 99709. Larry Freeman now retired
[2] Apatite to Zircon, Inc., 1075 Matson Rd., Viola, ID 83872; now at GeoSep Services, 1520 Pine Cone Rd, Moscow, ID 83843

A small number of detrital zircon analyses from the Ruby terrane have two distinct population patterns: one dominantly Mesoproterozoic and a second dominantly Paleoproterozoic (Bradley and others, 2007). In contrast, Rampart Group detrital zircon samples have dominant peaks in the Devonian (Bradley and others, 2007).

The U-Pb geochronologic data in this report complement previously released geochemical data (Lough and others, 2012) and geophysical data (Burns and others, 2010) from the Moran area; all data are incorporated into a geologic map (Freeman and others, 2022). The analytical data tables associated with this report are available in digital format as comma-separated value (CSV) files. See the accompanying metadata file for additional details about the organization of the digital files. All files can be downloaded from the DGGS website at https://doi.org/10.14509/31016.

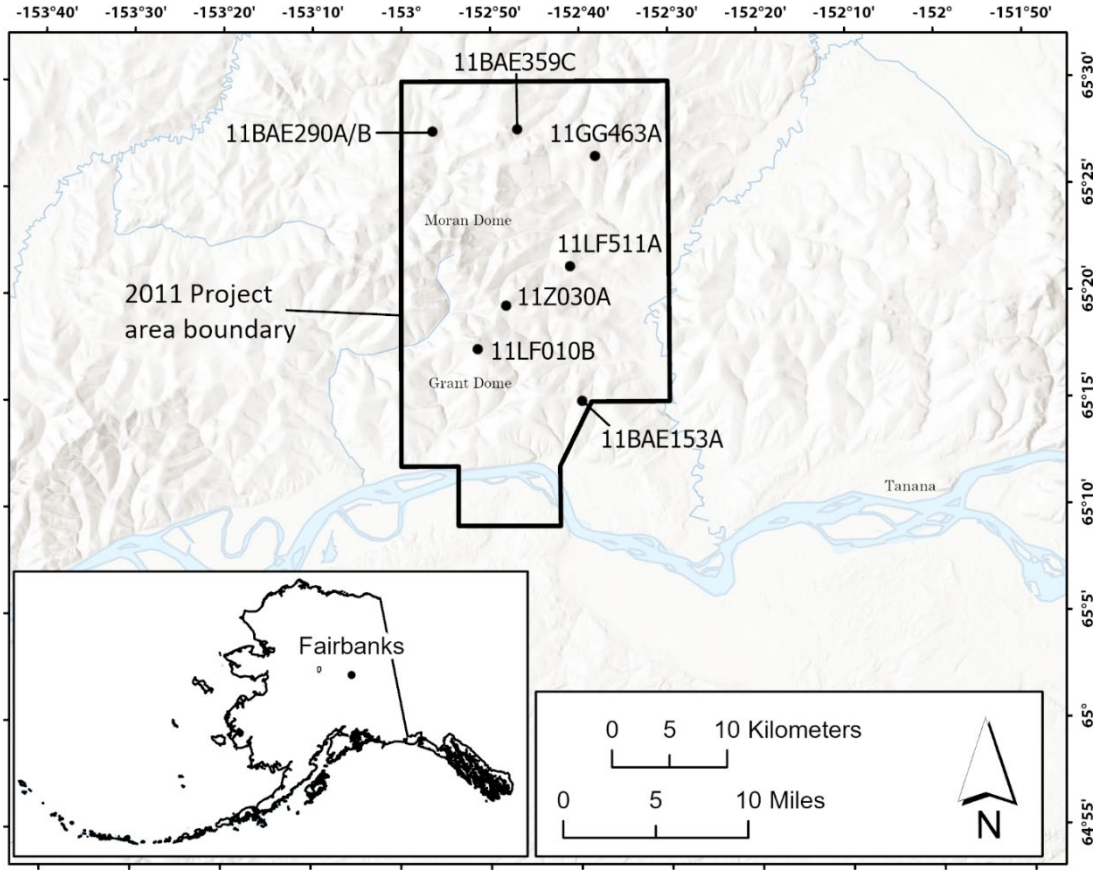

Figure 1. Map showing the 2011 project area with locations of U-Pb samples in this report.

DOCUMENTATION OF METHODS

Sample Collection

Rock samples collected during the 2011 DGGS field season were selected for two different purposes: (1) crystallization/cooling age of igneous rocks where rocks were selected to be representative of the rock type or intrusive body, and (2) detrital zircon ages where quartzite, quartz schist, or paragneiss were selected because they had relict clastic textures or were presumed to be metaclastic rocks from five distinct map units.

Location data for samples collected during the 2011 field campaign were derived using Garmin eTrex hand-held GPS units. Waypoints were downloaded from the eTrex units and merged with a hand-transcribed Microsoft Access field notes database daily, and locations were spot-checked to ensure the data merge was correct. Location error for the GPS units is estimated to range between 3 and 20 meters. The North American Datum (NAD) 1927 was used, and sample location coordinates are reported in NAD27 and World Geodetic System (WGS) 1984.

Zircon U-Pb Sample Preparation

Zircon grains were isolated and prepared for Laser Ablation-Inductively Coupled Plasma-Mass Spectrometry (LA-ICP-MS) analysis using standard procedures combined with specific customized procedures described by Donelick and others (2005). Whole rock samples were crushed using a jaw crusher with the minimum jaw separation set to 2–3 mm, sieved through 300 µm nylon mesh, and the <300 µm size fraction was washed with tap water and allowed to dry at room temperature. Zircon grains were separated from other mineral species using a combination of lithium metatungstate (density ~2.9 g/m^3), Frantz magnetic separator, diiodomethane (density ~3.3 g/cm^3), and hand-panning separation procedures. Epoxy wafers (~1 cm x 1 cm) containing zircon grains for LA-ICP-MS were polished manually using 3.0 µm and 0.3 µm Al_2O_3 slurries to expose internal zircon grain surfaces. The polished zircon grain surfaces were washed in 5.5 Molar (M) HNO_3 for 20 seconds at 21^0 C before introduction into the laser system sample cell.

Zircon U-Pb Sample analysis

LA-ICP-MS data collection was performed at the Geoanalytical Laboratory at Washington State University in Pullman, Washington. Individual zircon grains were targeted for data collection using a New Wave YP213 213 nm solid-state laser ablation system using a 20-µm-diameter laser spot size, 5 Hz laser firing rate, and ultra-high purity helium (He) as the carrier gas. Isotopic analyses of the ablated zircon material were performed using a ThermoScientific Element2 magnetic sector mass spectrometer using high-purity argon (Ar) as the plasma gas. The following masses (in atomic mass units [amu]) were monitored for 0.005 seconds (s) each in pulse-detection mode: ^{202}Hg, ^{204}(Hg +Pb), ^{206}Pb, ^{207}Pb, ^{208}Pb, ^{232}Th, ^{235}U, and ^{238}U. At time equal to 0.0 s, the mass spectrometer began monitoring signal intensities; at time equal to 6.0 s, the laser began ablating zircon material; at time equal to 30.0 s, the laser was turned off, and the mass spectrometer stopped monitoring signal intensities. A total of 250 data scans were collected for each zircon spot analyzed, comprising approximately 55 background scans, approximately 20 transition scans between background and background+signal, and approximately 175 background+signal scans. A scheme was developed to check whether ^{238}U experienced a switch from pulse to analog mode during data collection, and a correction procedure was employed to ensure the use of good-quality intensity data for masses ^{235}U and ^{238}U when such a switch was observed.

Zircon U-Pb Data Reduction

Previous LA-ICP-MS studies of U-Pb zircon dating used the so-called intercept method, which assumes that isotopic ratio varies linearly with scan number due solely to linearly varying isotopic fractionation (Chang and others, 2006; Gehrels and others, 2008). The data-modeling approach favored in this report was the modeling of background-corrected signal intensities for each isotope at each scan. Background intensity for each isotope was calculated using a fitted line (for decreasing background intensity) or using the arithmetic mean (for non-decreasing background intensity) at the global minimum of selected isotopes (^{206}Pb, ^{232}Th, and ^{238}U) for the spot. Background+signal intensity for each isotope at each scan was calculated using the median of fitted (2nd-order polynomial) intensity values for a moving window (seven scans wide here) that includes the scan. The precision of each background-corrected signal intensity value was calculated from the precision of the background intensity value and the precision of the background+signal intensity value.

U-Pb zircon age standards used during analysis are summarized in table 1, including the 1099.0 ± 0.6 Ma F.C. zircon (FC-1 of Paces and Miller, 1993) used here as the primary age standard. Isotopic data for F.C. were used to calculate Pb/U fractionation factors and their absolute errors for each F.C. data scan at each F.C. spot; these fractionation factors were smoothed session-wide for each data scan using the median of fitted (1st-order polynomial) fractionation factor values for a moving window (11 F.C. spots wide here) that includes the current F.C. spot and scan. Under the operating conditions of the LA-ICP-MS sessions in this study, fractionation factors were found to vary strongly with scan number, decreasing with increasing scan number (presumably due to increasing ablation pit depth and the effect this had on fractionation [Paton and others, 2010]). The zircon crystal lattice is widely known to accumulate α-radiation damage (Zhang and others, 2009, and references therein). It is assumed here that increased α-damage in a zircon leads to a decrease in the hardness of the zircon; this, in turn, leads to a faster rate of laser penetration into the zircon during ablation causing a dependence of isotopic fractionation on the degree of zircon lattice α-radiation damage. Ages calculated for all zircon age standards, when those standards were treated as unknowns, were used to construct a fractionation factor correction curve (exponential form) in terms of accumulated radiation damage. The notion of matrix-matched zircon standard and zircon unknown has been proposed largely based on trace element chemistry (Black and others, 2004). In this study, time and lattice damage parameters, invisible to instruments that characterize trace-element chemistry, were introduced and applied based on measured U and Th chemistries to effectively matrix-match standard and unknown zircon grains.

Uranium decay constants and the ^{238}U/^{235}U isotopic ratio reported in Steiger and Jäger (1977) were used in this study. Errors for the isotopic ratios ^{207}Pb/^{235}Uc (^{235}Uc = 137.88^{238}U), ^{206}Pb/^{238}U, and ^{207}Pb/^{206}Pb at each scan included errors from the background-corrected signal values for each isotope, the fractionation-factor error, and an additional relative error term required to force 95 percent of the F.C. ages to be concordant. Ages for the ratios ^{207}Pb /^{235}Uc, ^{206}Pb /^{238}U, and ^{207}Pb /^{206}Pb were calculated for each data scan and checked for concordance, defined as overlap of all three ages at the one sigma level (the use of two sigma level was found to skew the results to include scans with any significant common Pb). If the number of concordant data scans for a spot was greater than zero, the more precise age from the concordant-scan-weighted ratio ^{207}Pb /^{235}Uc, ^{206}Pb /^{238}U, or ^{207}Pb /^{206}Pb was chosen as the preferred age. Asymmetrical negative-direction and positive-direction age errors were calculated by subtracting and adding, respectively, the isotopic ratio errors in the appropriate age equation (Chew and Donelick, 2012).

Moving-median smoothing (MMS) is applied here to a subset (window) of *N* data points *x,y* of width *m* values of *x* to which a polynomial of order *n* is fitted. For each value of *x* at each position of the data window, a value of *y* is calculated for the fitted polynomial. The window is positioned with the right-hand boundary at the left-hand *x* value and then shifted *N-1* times until the left-hand boundary of the window is positioned at the right-hand *x* value. At each *x* position, *m* fitted values of *y* are calculated, and the median of these fitted values is taken.

Table 1. Zircon age standards used during this analysis.

Standard	Standard	U-Pb age (± 2σ)	Reference
F.C.	Duluth complex	1,099.0 ± 0.6 Ma	Paces and Miller, 1993
F5	Duluth complex	1,099.0 ± 0.6 Ma (assumed equal to FC-1)	Paces and Miller, 1993
IF	Fish Canyon Tuff	28.201 ± 0.012 Ma	Lanphere and Baadsraard, 2001; Kuiper and others, 2008
MD	Mount Dromedary	99.12 ± 0.14 Ma	Renne and others, 1998
PX	Peixe	563.5 ± 1.6 Ma	Gehrels and others, 2008
R3	Braintree complex	418.9 ± 0.4 Ma	Black and others, 2004
T2	Temora 2, Middledale gabbroic diorite	416.78 ± 0.33 Ma	Black and others, 2004
TR	Tardree Rhyolite	61.23 ± 0.11 Ma	Dave Chew, pers. commun.

Zircon U-Pb Data Interpretation

The digital data accompanying this report provide sample locations, age summaries for each sample, and all the U-Pb experiment (analysis) results for individual zircon grains in each sample (table 2). Individual zircon $^{207}Pb/^{235}U$, $^{206}Pb/^{238}U$, and $^{207}Pb/^{206}Pb$ ages are quoted to the ±2 sigma level as reported by Apatite to Zircon, Inc. (A to Z).

Individual zircon $^{207}Pb/^{235}U$, $^{206}Pb/^{238}U$, $^{207}Pb/^{206}Pb$, and concordia ages and uncertainties at the ±2 sigma level were also calculated from measured isotopic ratios using IsoplotR (Vermeesch, 2018) with the same decay constants and ratios used by A to Z. The concordia age is calculated as the maximum likelihood intersection between the (Wetherill) concordia line and the ($^{207}Pb/^{235}U$- and $^{206}Pb/^{238}U$-ratio) error ellipse. Discordance of each grain was determined using two methods: concordia distance (percent), measured along a line connecting the measured composition and the corresponding single grain concordia age composition (Veermesch, 2021), and relative age difference (percent) measured as the ratio of $^{206}Pb/^{238}U$ to $^{207}Pb/^{206}Pb$ ages.

Individual zircon ages with high uncertainty (greater than 10 percent uncertainty in either direction), ages using lead-corrected isotopic ratios, and analyses with anomalously low uranium were omitted in multi-grain age interpretations and on plots. Individual grains with high discordance and manually identified ages are omitted in weighted-mean or concordia age calculations but are depicted

in the weighted-mean and concordia plots. Omitted grains are identified in the data as follows: individual analyses marked as (lowercase) 'x' are plotted (except on kernel density estimate [KDE] and histogram plots) but ignored for numerical analysis, and individual grains marked as (uppercase) 'X' are omitted from both plots and calculations. The criteria used for each individual analysis omission are listed in the data tables.

For samples where a single crystallization age was targeted, composite weighted-mean ages and composite concordia ages were calculated with IsoplotR, v.5.1 (Veermesch, 2018). Weighted-mean plots and age determinations use the individual grain $^{206}Pb/^{238}U$ ages, screened for discordance using concordia distance values of -3.5 and 16 percent. Ages that were distinctly out of the main population were manually omitted as well. In the weighted-mean age calculations, outliers were eliminated using a modified Chauvenet outlier detection criteria (Veemeesch, 2018). Common lead corrections and disequilibrium corrections were not used. Analytical uncertainty associated with decay constants and calibration factors were propagated into the age. The analytical uncertainty of crystallization ages is presented at two standard deviations (also written as two-sigma or 2σ), with the final uncertainties consisting of random and systematic uncertainties added in quadrature. Uncertainties for the ages reported in table 2 and in the text below include both analytical and systematic sources of uncertainty. We assumed a systematic uncertainty factor of two percent ($^{206}Pb/^{238}U$) following the example of Wildland and others (2022).

Samples collected for detrital zircon maximum depositional age (MDA) and provenance use the individual $^{206}Pb/^{238}U$ age (if less than 1.5 billion years [Ga]), or the $^{207}Pb/^{206}Pb$ age (if greater than 1.5 Ga) screened for discordance using relative age difference values of -10 and 30 percent and concordia distance values of -3.5 and 16 percent. Following the example of Twelker and O'Sullivan (2021), the MDA of each sample used the youngest statistical population (YSP) approach of Coutts and others (2019). A YSP MDA is the weighted mean of two or more of the youngest zircon grains that yield a mean square weighted deviation (MSWD) closest to 1.0; these weighted-mean dates were calculated using a spreadsheet developed by Boise State University Isotope Geology Laboratory (Herriott and others, 2019). Uncertainties for the YSP MDAs reported in table 2 include both analytical and systematic sources of uncertainty; these uncertainties were propagated into the total uncertainty by quadrature. We assumed a systematic uncertainty factor of two percent($^{206}Pb/^{238}U$) of Twelker and O'Sullivan (2021). Overall, individual age populations are displayed with Wetherill concordia diagrams, age-ranked weighted-mean plots, and combined age histograms and KDE plots using IsoplotR (Vermeesch, 2018). The histogram bin width is 50 Ma; adaptive kernel bandwidth was used for the KDE plots.

Table 2. Summary of best ages (the weighted-mean age representing crystallization or YSP to establish MDAs) of analyzed zircon samples. Map units correspond to those in Freeman and others' (2022) geologic map of the eastern Moran area.

Sample	Map Unit	Lithology	Latitude (NAD27)	Longitude (NAD27)	Best age (Ma) ± 2σ	YSP (Ma) ± 2σ	MSWD
11BAE290A	Kgr	Granite	65.461	-152.942	111.7 ± 2.3	-	5.8
11BAE290B	Kgr	Aplitic granite	65.461	-152.942	114.4 ± 2.3	-	5.1
11BAE359C	Kgr	Rhyolite dike	65.463	-152.782	113.2 ± 2.4	-	6.1
11BAE153A	|<fs	Schist	65.251	-152.663	-	1128.3 ± 27.4	2.6
11GG463A	Dq	Metaconglomerate	65.442	-152.640	-	365.9 ± 8.7	0.7
11LF010B	|<gn	Paragneiss	65.392	-153.082	-	928.3 ± 27.1	0.8
11LF511	Mq	Quartz schist	65.357	-152.685	-	450.7 ± 10.8	1.5
11Z030A	Dvs	Schist	65.325	-152.805	-	324.8 ± 7.7	0.3

RESULTS

Below, we briefly discuss the results of each sample analysis from the Moran area (Freeman and others, 2022). The first three samples were collected to obtain the crystallization age of the Melozitna pluton. The remaining five samples were collected for detrital zircon MDA and provenance age populations.

11BAE290A – Granite of the Melozitna pluton (Kgr)

A total of 118 zircon grains from 11BAE290A were successfully analyzed; 86 were used for the weighted mean and 87 for concordia ages (fig. 2). The concordia age (112.5 ± 2.3 Ma) and the weighted mean age (111.7 ± 2.3 Ma) are within error. We prefer the weighted mean age because of the lower MSWD. This age represents the crystallization age of the coarse-grained granite at this outcrop. A $^{40}Ar/^{39}Ar$ plateau age of 116.5 ± 1.3 Ma was obtained on a biotite mineral separate from the same sample (Benowitz and others, 2019).

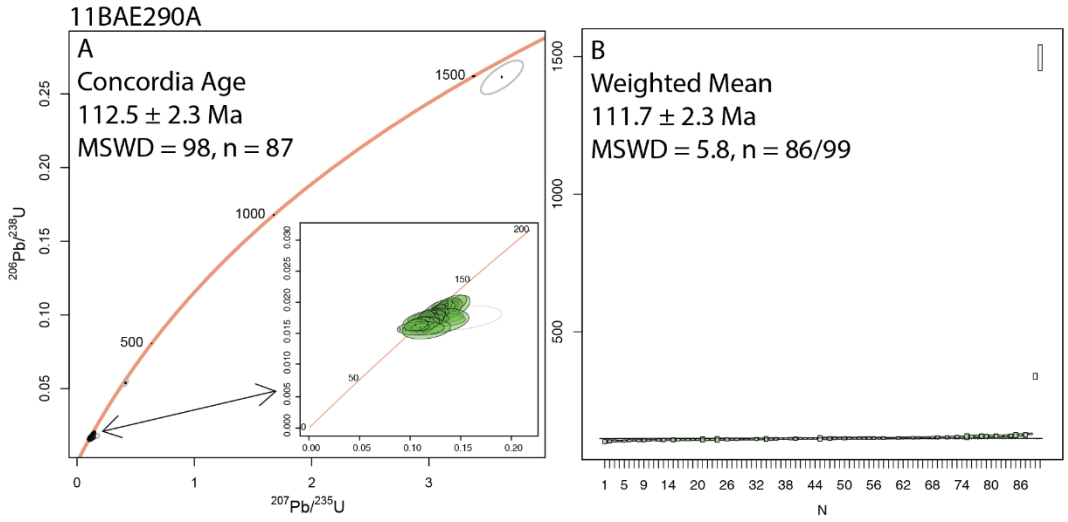

Figure 2. U-Pb plots for sample 11BAE290A. **A.** Concordia diagram and concordia age. Ellipses represent two-sigma errors; filled ellipses are concordant grains used in the age calculations. **B.** Ranked age weighted mean diagram. Bars indicate the two-sigma uncertainty range of individual ages; closed bars are concordant ages that were used in the age calculation. Age uncertainty in both figures includes both two-sigma uncertainty and a two percentsystematic uncertainty.

11BAE290B – Aplitic granite of the Melozitna pluton (Kgr)

A total of 120 zircon grains extracted from sample 11BAE290B were successfully analyzed; 21 were rejected, and 93 were used for both the concordia age of 114.8 ± 2.3 and the weighted-mean age of 114.4 ± 2.3 Ma (fig. 3). The two ages are within error. We prefer the weighted mean age because of the lower MSWD. This age represents the crystallization age of the fine-grained leucocratic granite, which occurs in contact with the coarse-grained granite (11BAE290A). A $^{40}Ar/^{39}Ar$ plateau age of 110.1 ± 1.3 Ma was obtained on a biotite mineral separate from the same sample (Benowitz and others, 2019).

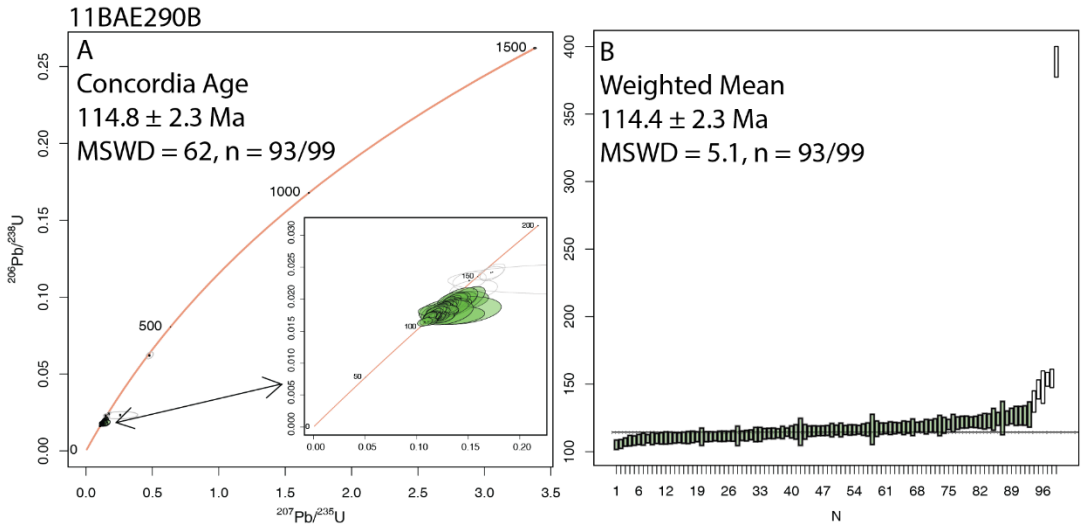

Figure 3. U-Pb plots for sample 11BAE290B. **A.** Concordia diagram and concordia age. Ellipses represent a two-sigma error; filled ellipses are concordant grains used in the age calculations. **B.** Ranked age weighted mean diagram and age. Bars indicate the two-sigma uncertainty range of individual ages; closed bars are concordant ages that were used in the age calculation. Age uncertainty in both figures includes both two-sigma uncertainty and a two percentsystematic uncertainty.

11BAE359C – Porphyry rhyolite dike of Melozitna pluton (Kgr)

A total of 79 zircon grains from sample 11BAE359C were analyzed; 22 analyses were rejected, and five were anomalously old. The remainder constitutes a bimodal population (fig. 4), which can be explained by field sampling error. The larger population of 48 zircon grains is included in a concordia age of 114.6 ± 2.4 Ma (fig. 4A) and 41 zircon grains in a weighted-mean age of 113.2 ± 2.6 Ma (fig. 4C). We prefer the weighted-mean age because of the lower MSWD. A second population, not included in table 2, of six analyses yields a concordia age of 56.7 ± 1.6 Ma (fig. 4B) and five zircon grains in a weighted-mean age of 55.9 ± 1.7 (fig. 4D). A $^{40}Ar/^{39}Ar$ plateau age of 102.8 ± 1.2 Ma was obtained on aphanitic groundmass from the same sample (Benowitz and others, 2019). The material for the U-Pb sample was a composite collected from frost-fractured rubble at the base of an outcrop of coarse-

grained phaneritic granite, whereas the $^{40}Ar/^{39}Ar$ sub-sample was selected from a single specimen of the frost-fractured material. Field notes indicate two similar varieties of porphyritic rhyolite are represented in the frost-fractured material. It is conceivable that the sub-sample submitted for U-Pb zircon ages is an admixture of two parallel dikes: one with the age of 113.2 Ma, consistent with samples 11BAE290A and 11BAE290B and with $^{40}Ar/^{39}Ar$ ages of 102.8 to 116.5 Ma (Benowitz and others, 2019) from the Melozitna pluton, and the second, with an age of 56.9 Ma, within the range of K/Ar ages of volcanic and sub-volcanic rocks mapped elsewhere along the southeast margin of the Koyukuk basin in the northern Melozitna and Tanana quadrangles (units Ta, Tad, and Td in Patton and others, 2009).

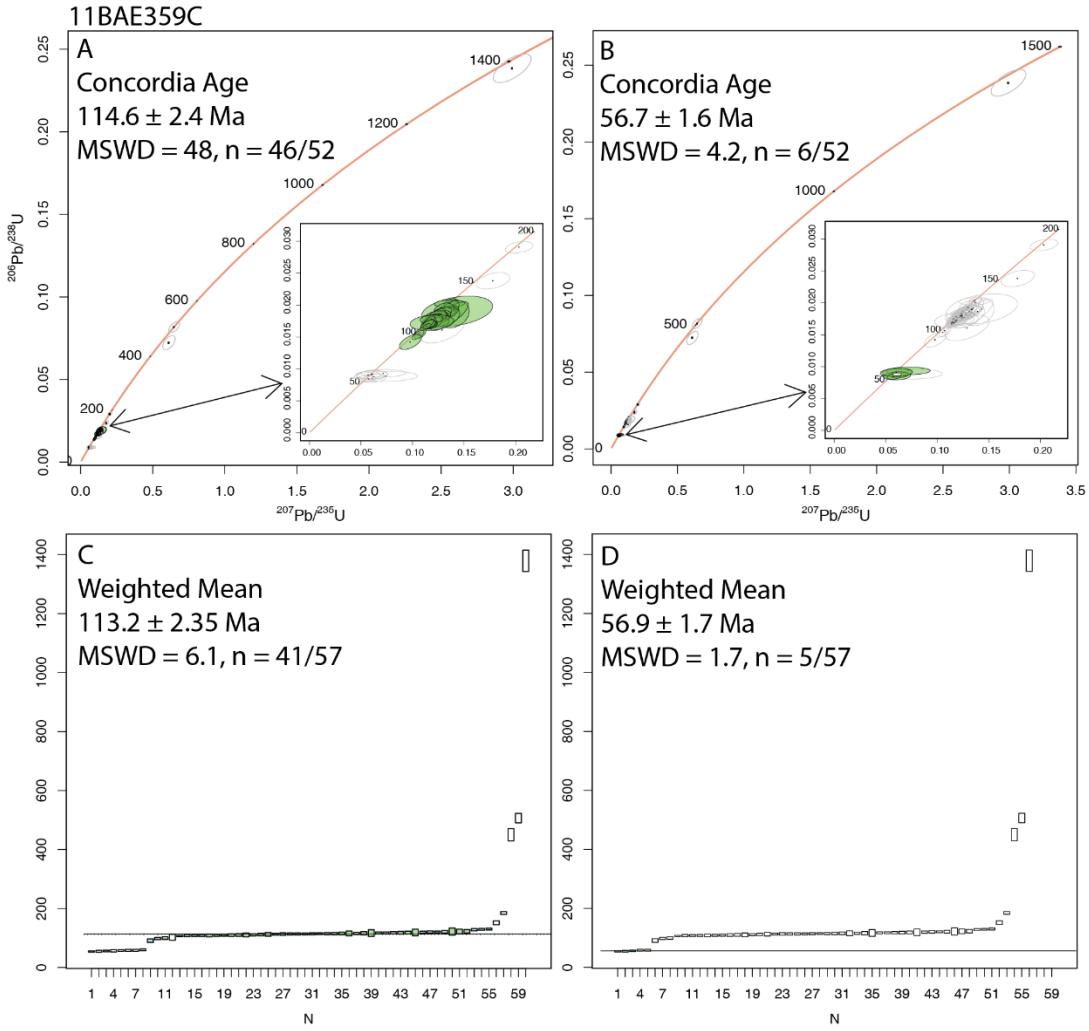

Figure 4. U-Pb plots for sample 11BAE359C. **A.** Concordia diagram and concordia age. Ellipses represent a two-sigma error; filled ellipses are concordant grains used in the age calculations. **B.** Concordia diagram and age for a population of zircon grains interpreted as contamination from a younger dike. **C.** Ranked age weighted mean diagram and age. Bars indicate the two-sigma uncertainty range of individual ages; closed bars are concordant ages that were used in the age calculation. **D.** Ranked age weighted mean diagram for a population of zircon grains interpreted as contamination from a younger dike. Age uncertainty in all diagrams includes two-sigma uncertainty and a two percent systematic uncertainty.

11BAE153A – Schist of the Ruby terrane (Unit |<fs)

A total of 116 zircon grains from sample 11BAE153A were successfully analyzed; 81 concordant zircon grains were used in the KDE and histogram plot (figs. 5A, B). The YSP of 1128.3 ± 27.4 used four analyses (fig. 5C). The youngest single zircon has an age of 971.6 ± 31.8 Ma. The age population has major clusters from 1,750 to 2,050 Ma (37 zircon grains) and from 2,450 to 2,650 Ma (17 zircon grains), a secondary cluster from 2,150 to 2,400 Ma (11 zircon grains), and two minor clusters from 1,100 to 1,200 Ma and 1,400 to 1,500 Ma (4 zircon grains each). The predominance of Paleoproterozoic zircon grains in this sample closely resembles a sample of quartzite from the Ruby terrane and detrital zircon populations from the Wickersham Grit in the Yukon-Tanana terrane (Bradley and others, 2007); by extension, this sample (map unit |<fs; Freeman and others, 2022) likely has a North American provenance.

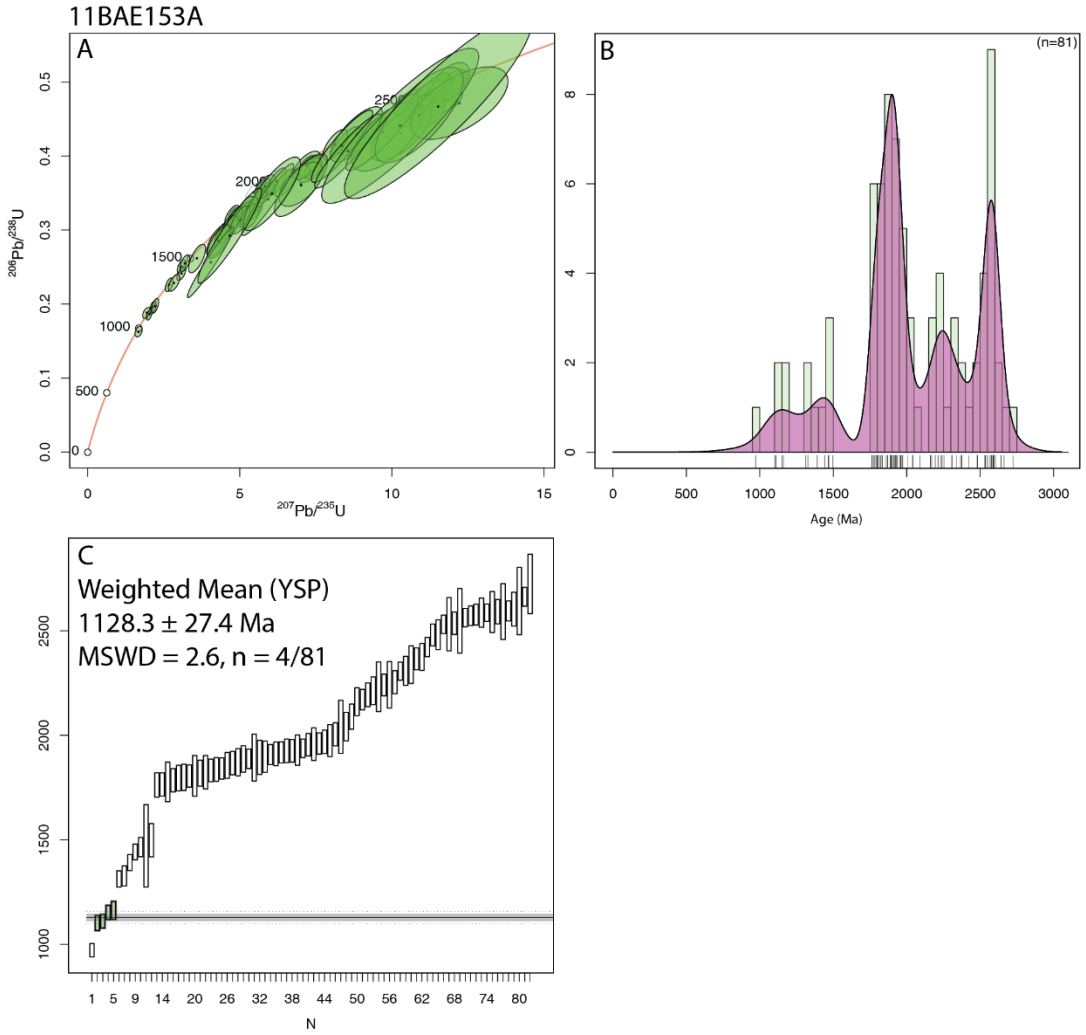

Figure 5. U-Pb plots for sample 11BAE153A. **A.** Concordia diagram. Ellipses represent two-sigma error; filled ellipses are concordant grains. **B.** Kernel density estimate plot and histogram of concordant analyses of detrital zircon grains. The histogram bin width is 50 Ma. **C.** Ranked age weighted mean diagram illustrating the youngest statistical population. Bars indicate the two-sigma uncertainty range of individual ages; closed bars are concordant ages that were used in the age calculation. Age uncertainty includes both two-sigma uncertainty and a two percent systematic uncertainty.

11GG463A – Stretched-pebble conglomerate (Unit Dq)

A total of 20 zircon grains were successfully analyzed from 11GG463A. Seventeen concordant scans were used in the KDE and histogram plot (fig. 6A, B). The age of the youngest concordant grain (71.6 Ma) is geologically incompatible and may represent contamination introduced during sample selection or preparation. The second-youngest grain (146.5 Ma) is consistent with the prograde metamorphism of the Ruby and Tozitna Terranes (Roeske and others, 1995; Benowitz and others, 2019) or may represent sample contamination. The YSP is 365.9 ± 8.7 Ma and represents the MDA of the sample (fig. 6C). A second population of five grains has a weighted-mean age of 432.0 ± 10.7 Ma (fig. 6D). The remaining four zircon grains are Neoproterozoic and Paleoproterozoic.

Figure 6. U-Pb plots for sample 11GG463A. **A.** Concordia diagram. Ellipses represent two-sigma error; filled ellipses are

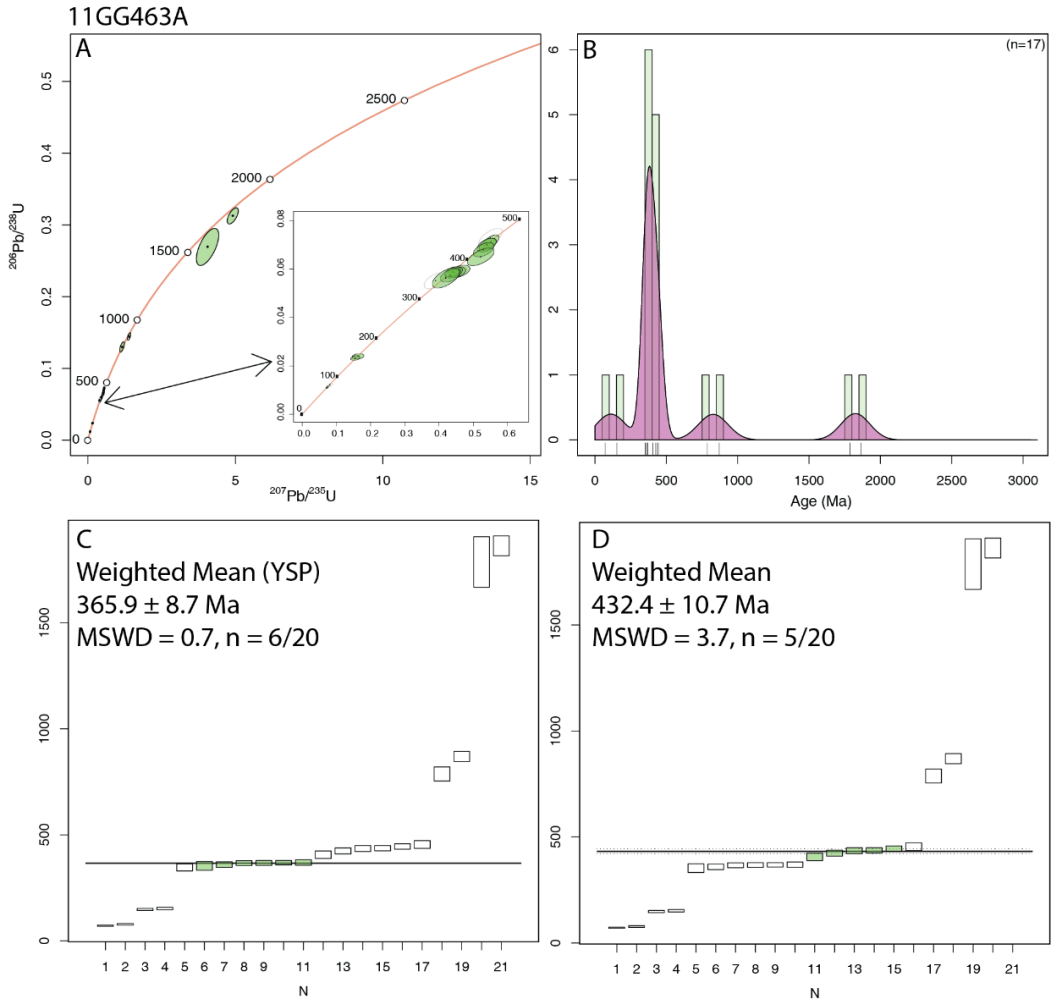

concordant grains. **B.** Kernel density estimate plot and histogram of concordant analyses of detrital zircon grains. The histogram bin width is 50 Ma. **C.** Ranked age weighted mean diagram that illustrates the youngest statistical population. Bars indicate the two-sigma uncertainty range of individual ages; closed bars are concordant ages that were used in the age calculation. **D.** Ranked age weighted mean diagram illustrating a second significant population. Bars indicate the two-sigma uncertainty range of individual ages; closed bars are concordant ages that were used in the age calculation. Age uncertainty in (**C**) and (**D**) includes two-sigma and two percent systematic uncertainty.

11LF010B – Paragneiss of the Ruby terrane (Unit |<gn)

A total of 54 zircon grains were successfully analyzed from 11LF010B, a paragneiss from within the contact-metamorphic aureole of the Melozitna pluton. Many (24) individual grain analyses were rejected, likely because of contact metamorphism. A total of 28 concordant grains are plotted on the diagrams (figs. 7A, B). The YSP is 928.3 ± 27.1 Ma and represents the MDA of the sample (fig. 7C). Most of the concordant grains (21) fall in a broad cluster from 1,407 to 1,932 Ma, another six zircon grains form a secondary cluster from 950 to 1,150 Ma. Most Mesoproterozoic zircon grains in this sample closely resemble detrital zircon samples of quartzite from the Ruby terrane at Senatis Creek and Illinois Creek and of a sample from the Minook quartzite (Bradley and others, 2007).

Figure 7. U-Pb plots for sample 11LF010B. **A.** Concordia diagram. Ellipses represent two-sigma error; filled ellipses are

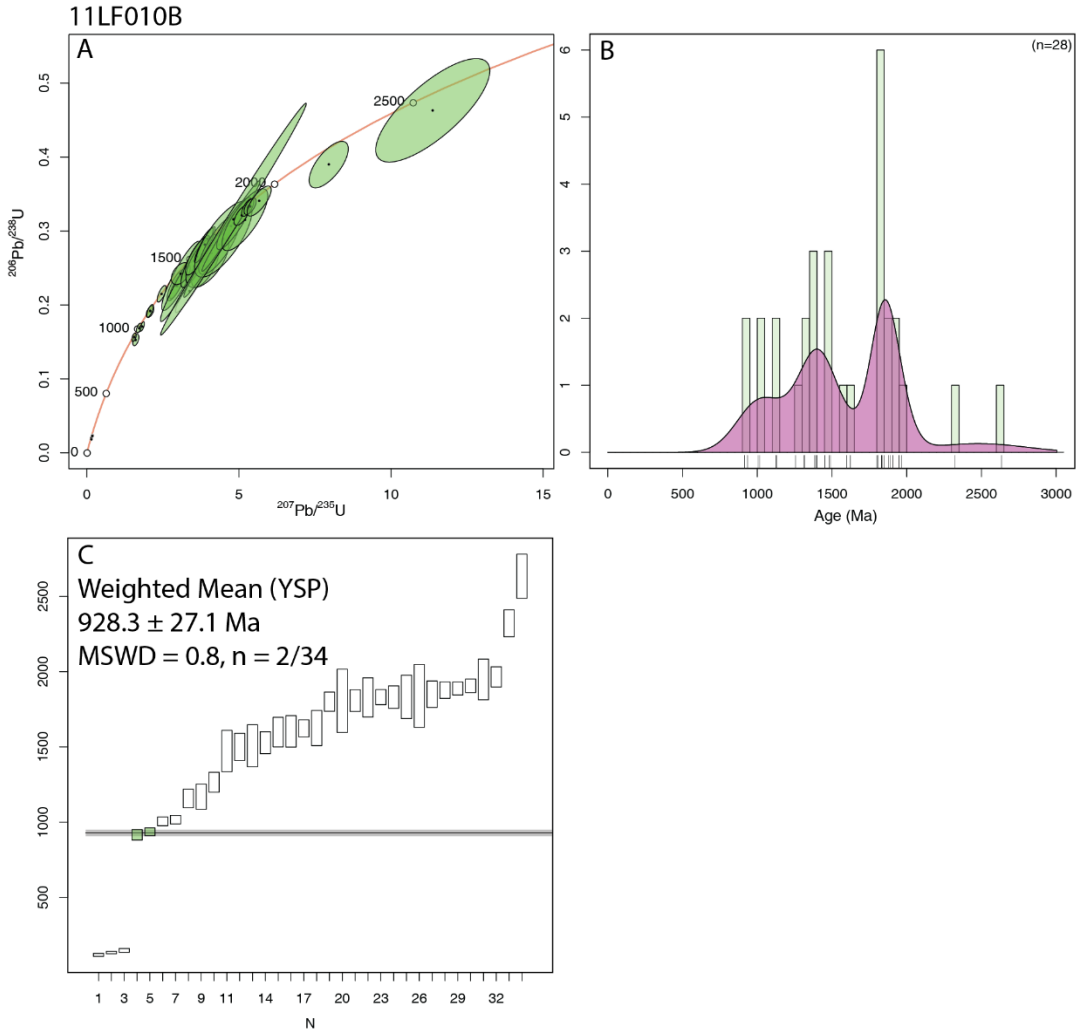

concordant grains. **B.** Kernel density estimate plot and histogram of concordant analyses of detrital zircon grains. The histogram bin width is 50 Ma. **C.** Ranked age weighted mean diagram illustrating the youngest statistical population. Bars indicate the two-sigma uncertainty range of individual ages; closed bars are concordant ages that were used in the age calculation. Age uncertainty includes both two-sigma uncertainty and a two percent systematic uncertainty.

11LF511A – Quartzite of the Ruby terrane (Unit Mq)

A total of 37 grains were analyzed from 11LF511A, a black-banded quartzite. Several individual analyses (13) had anomalously low uranium and were omitted. The youngest concordant grain has an age of 329.4 ± 10.7 Ma (figs. 8A, B). The remaining six concordant zircon grains form a single population with a weighted mean age of 450.7 ± 10.8 Ma (fig. 8C). We believe that the youngest single zircon is likely closer to the MDA of this sample than the YSP because of the small number of concordant zircon grains recovered.

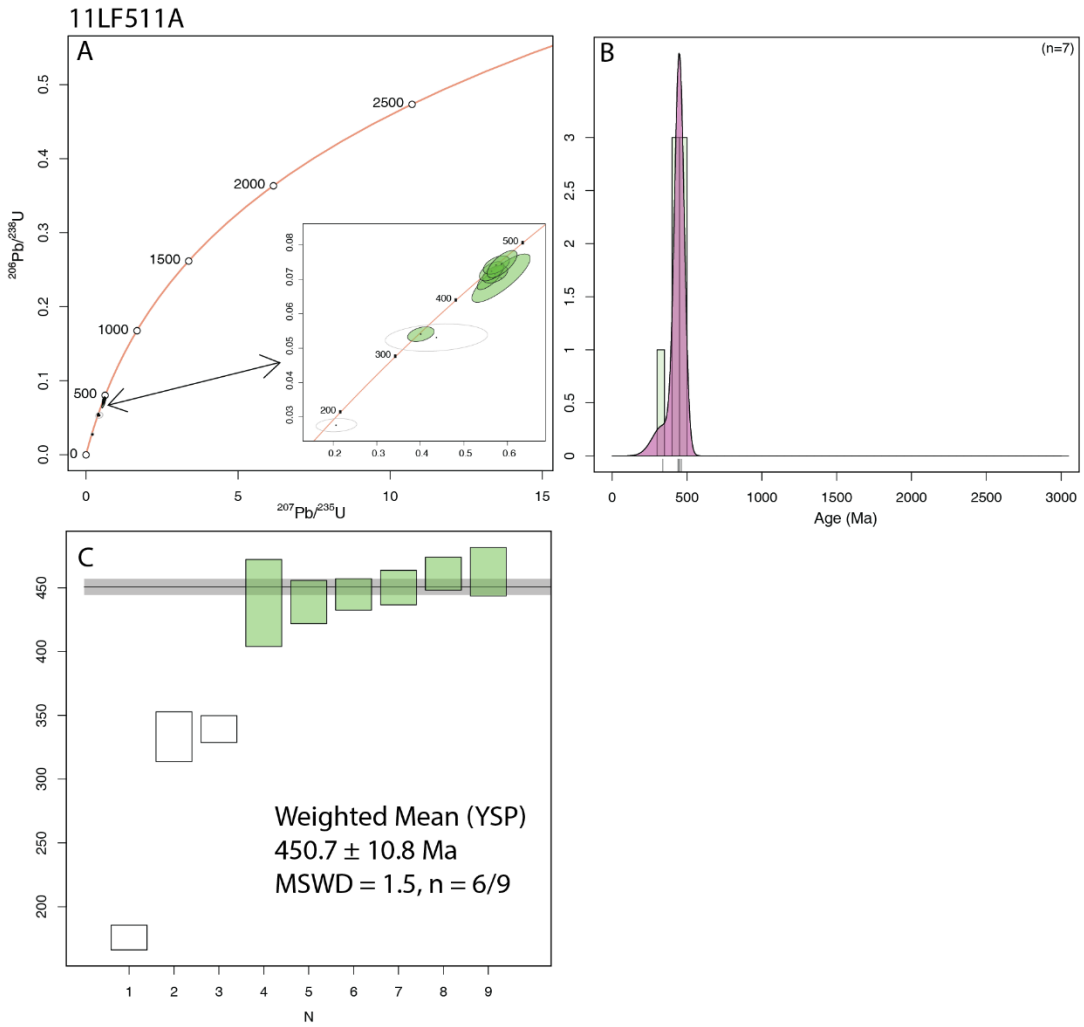

Figure 8. U-Pb plots for sample 11LF511A. **A.** Concordia diagram. Ellipses represent two-sigma error; filled ellipses are concordant grains. **B.** Kernel density estimate plot and histogram of concordant analyses of detrital zircon grains. The histogram bin width is 50 Ma. **C.** Ranked age weighted mean diagram illustrating the youngest statistical population. Bars indicate the two-sigma uncertainty range of individual ages; closed bars are concordant ages that were used in the age calculation. Age uncertainty includes both two-sigma uncertainty and a two percent systematic uncertainty.

11Z030A – Schist of the Ruby terrane (Unit Dvs)

A total of 116 zircon grains were successfully analyzed from 11Z030A. Eight out of 106 concordant individual analyses (fig. 8A, B) comprise the YSP with a weighted mean age of 324.8 ± 7.7 (fig. 8C) and represent the MDA. The YSP is part of a much broader population (near 440 Ma on KDE) of 54 zircon grains with a weighted mean age of 360.6 ± 7.5 Ma (fig. 8D). The KDE diagram (fig. 8B) shows that older Paleozoic ages skew this peak. A secondary peak comprised of 23 analyses falls between 1,600 and 1,850 Ma, and seven other zircon grains fall in a third population between 750 and 900 Ma. The age of this map unit (Freeman and others, 2022) should be reinterpreted to be Mississippian. The Paleozoic populations of zircon grains yielded in samples 11Z030A and 11LF511A suggest that the two map units are part of a larger group. The Neoproterozoic and Mesoproterozoic populations are like those in 11LF010B.

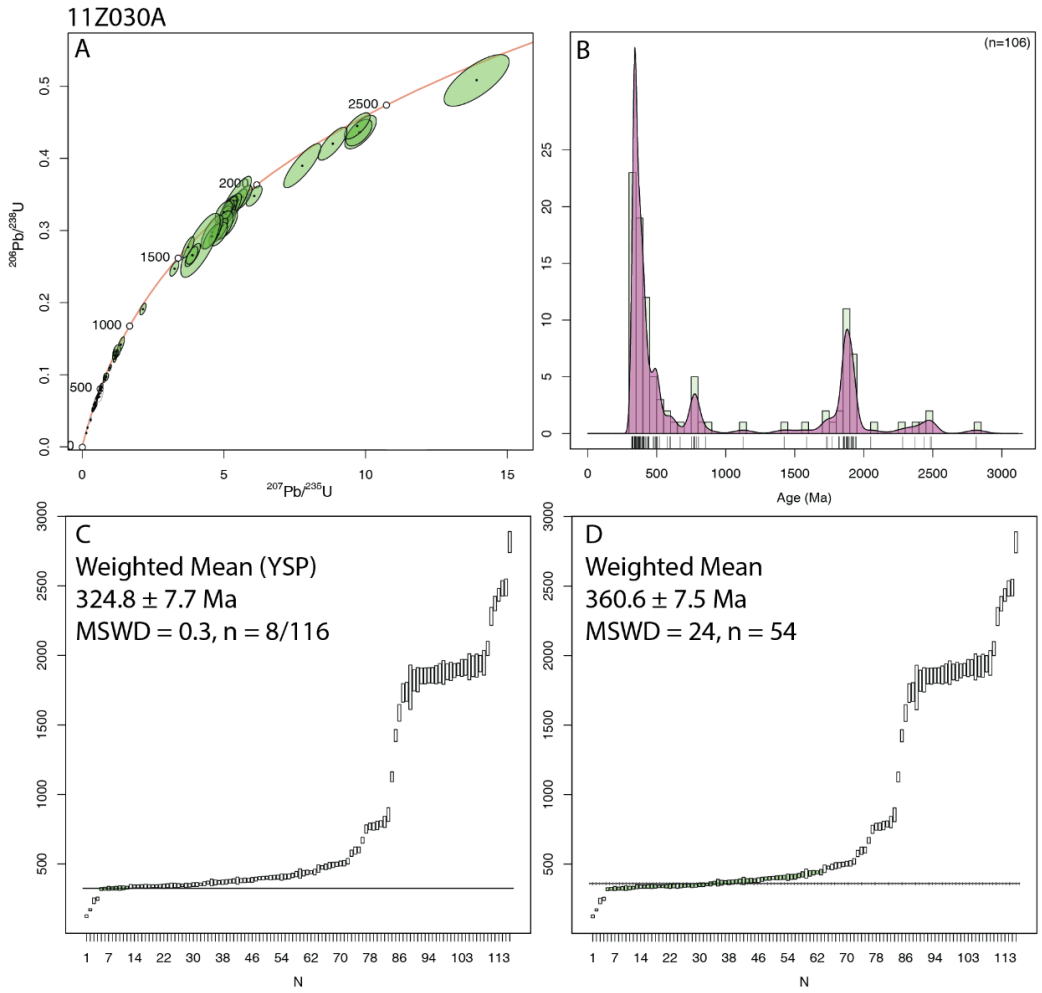

Figure 9. U-Pb plots for sample 11Z030A. **A.** Concordia diagram. Ellipses represent two-sigma error; filled ellipses are concordant grains. **B.** Kernel density estimate plot and histogram of concordant analyses of detrital zircon grains. The histogram bin width is 50 Ma. **C.** Ranked age weighted mean diagram illustrating the youngest statistical population. Bars indicate the two-sigma uncertainty range of individual ages; closed bars are concordant ages that were used in the age calculation. **D.** Ranked age weighted mean diagram illustrating the population of this sample's largest range of zircon

grains. Bars indicate the two-sigma uncertainty range of individual ages; closed bars are concordant ages that were used in the age calculation. Age uncertainty in (C) and (D) includes two-sigma and two percent systematic uncertainty.

ACKNOWLEDGMENTS

The authors wish to thank the following individuals: Margaret Donelick and Jim McMillan (Apatite to Zircon, Inc.) for technical assistance regarding sample preparation; Charles Knaack (Washington State University) for technical assistance regarding LA-ICP-MS data collection; and Paul O'Sullivan and Ray Donelick (Apatite to Zircon, Inc.) for assistance with LA-ICP-MS data interpretation.

Concordia diagrams, ranked-date weighted-mean plots, and kernel density estimates were created using the free online version of IsoplotR (Vermeesch, 2018). Mark Schmitz kindly provided his spreadsheet for calculating the youngest statistical population ages of detrital zircon grains (Herriot and others, 2019). Evan Twelker assisted the authors in processing the data to be compatible with current DGGS practices. Doyon Limited owns part of the land in the 2019 DGGS study area, including the site of sample 11BAE153A; we thank them for permission to work on these lands.

This project is part of the Alaska Airborne Geophysical/Geological Mineral Inventory program funded by the Alaska State Legislature and managed by the State of Alaska, Department of Natural Resources, Division of Geological & Geophysical Surveys. The State of Alaska General Fund and the U.S. Geological Survey's STATEMAP Program under award number G11AC20203 also provided partial funding for the geologic mapping and geochemical analyses. The views and conclusions contained in this document are those of the authors and should not be interpreted as representing the opinions or policies of the U.S. Geological Survey. Mention of trade names or commercial products does not constitute their endorsement by the U.S. Geological Survey.

REFERENCES

Barker, James, and Warner, Dean, 1985, Investigation of Tozimoran placers field report, October 1985: U.S. Bureau of Mines Field Report, 4 p. https://dggs.alaska.gov/pubs/id/23064

Black, L.P., Kamo, S.L., Allen, C.M., Davis, D.W., Aleinikoff, J.N., Valley, J.W., Mundil, Roland, Campbell, I.H., Korsch, R.J., Williams, I.S., and Foudoulis, Chris, 2004, Improved $^{206}Pb/^{238}U$ microprobe geochronology by the monitoring of trace-element-related matrix effect—SHRIMP, ID-TIMS, ELA-ICP-MS, and oxygen isotope documentation for a series of zircon standards: Chemical Geology, v. 205, p. 15–140.

Benowitz, J.A., Layer, P.W., Freeman, L.K., Griesel, G.A., Elliott, B.A., Szumigala, D.J., Wypych, Alicja, and Montayne, Simone, 2019, $^{40}Ar/^{39}Ar$ data from the eastern Moran area, Tanana B-6 and C-6 quadrangles, and the Ruby mining district, Ruby B-5 and B-6 quadrangles, Alaska: Alaska Division of Geological & Geophysical Surveys Raw Data File 2018-5, 28 p. https://doi.org/10.14509/30117

Bradley, D.C., McClelland, W.C., Wooden, J.L., Till, A.B., Roeske, S.M., Miller, M.L., Karl, S.M., and Abbott, J.G., 2007, Detrital zircon geochronology of some Neoproterozoic to Triassic rocks in interior Alaska, *in* Ridgway, K.D., Trop, J.M., Glen, J.M.G., and O'Neill, J.M., eds., Tectonic Growth of a Collisional Continental Margin: Crustal Evolution of Southern Alaska: Geological Society of America Special Paper 431, p. 155–189.

Burns, L.E., Fugro Airborne Surveys Corp., and Stevens Exploration Management Corp., 2010, Line, grid, and vector data, and maps for the airborne geophysical survey of the Moran Survey Area, Melozitna and Tanana quadrangles, central Alaska: Alaska Division of Geological & Geophysical

Surveys Geophysical Report 2010-1, 56 sheets, scale 1:63,360, 1 DVD. http://doi.org/10.14509/20561

Chang, Zhaoshan, Vervoort, J.D., McClelland, W.C., and Knaack, Charles, 2006, U-Pb dating of zircon by LA-ICP-MS: Geochemistry, Geophysics, Geosystems, American Geophysical Union, v. 7, n. 5, 14 p. https://doi.org/10.1029/2005GC001100

Chapman, R.M., Coats, R.R., and Payne, T.G., 1963, Placer tin deposits in central Alaska: U.S. Geological Survey Open File Report: Technical Data Unit classification number 239, 53 p., 10 sheets.

Chapman, R.M., Yeend, Warren, Brosge, W.P., and Reiser, H.N., 1982, Reconnaissance geologic map of the Tanana Quadrangle, Alaska: U.S. Geological Survey Open-File Report 82-734, 18 p., 1 sheet, scale 1:250,000.

Chew, D.M., and Donelick, R.A., 2012, Combined apatite fission track and U-Pb dating by LA-ICP-MS and its application in apatite provenance analysis: Mineralogical Association of Canada Short Course, v. 42, p. 219–247.

Coutts, D.S., Matthews, W.A., and Hubbard, S.M., 2019, Assessment of widely used methods to derive depositional ages from detrital zircon populations: Geoscience Frontiers, v. 10, n. 4, p. 1,421–1,435. https://doi.org/10.1016/j.gsf.2018.11.002

Donelick, R.A, O'Sullivan, P.B., and Ketcham, R.A., 2005, Apatite fission-track analysis: Reviews in Mineralogy and Geochemistry, Mineralogical Society of America, v. 58, p. 49–94.

Freeman, L.K., Newberry, R.J., Griesel, G.A., Elliott, B.A., Lough, T.A., and Twelker, Evan, 2022, Bedrock geologic map of the eastern Moran area, Tanana B-6 and C-6 quadrangles, Alaska: Alaska Division of Geological & Geophysical Surveys Raw Data File 2022-11, 16 p. https://doi.org/10.14509/30884

Gehrels, G.E., Valencia, V.A., and Ruiz, J., 2008, Enhanced precision, accuracy, efficiency, and spatial resolution of U-Pb ages by laser ablation–multicollector–inductively coupled plasma–mass spectrometry: Geochemistry Geophysics Geosystems, American Geophysical Union, v. 9, 13 p.

Herriott, T.M., Crowley, J.L., Schmitz, M.D., Wartes, M.A., and Gillis, R.J., 2019, Exploring the law of detrital zircon; LA-ICP-MS and CA-TIMS geochronology of Jurassic forearc strata, Cook Inlet, Alaska, USA: Geology, v. 47, p. 1,044–1,048. https://doi.org/10.1130/G46312.1

International Tower Hill Mines, Ltd, 2006, ITH confirms presence of a major gold target on its West Tanana Project, Alaska [Press Release]. Retrieved on May 3, 2010 from: http://www.ithmines.com/s/NewsReleases.asp?ReportID=157834&_Ty

International Tower Hill Mines, Ltd, 2007, ITH reports initial drilling results at West Tanana Project, central Alaska [Press Release]. Retrieved on May 3, 2010 from: http://www.ithmines.com/s/NewsReleases.asp?ReportID=209034&_Ty

Kuiper, K.F., Deino, A., Hilgen, P.J., Krijgsman, W., Renne, P.R., and Wijbrans, J.R., 2008, Synchronizing rock clocks of Earth history: Science, v. 320, p. 500–504.

Lanphere, M.A. and Baadsraard, H., 2001. Precise K-Ar, $^{40}Ar/^{39}Ar$, Rb-Sr and U-Pb mineral ages from the 27.5 Ma Fish Canyon Tuff reference standard. Chemical Geology, v. 175, p. 653-671.

Lough, T.A., Freeman, L.K., Elliott, B.A., Griesel, G.A., Newberry, R.J., and Szumigala, D.J., 2012, Geochemical, major-oxide, minor-oxide, trace-element, and carbon data from rocks collected in 2011 in the Moran area, Tanana and Melozitna quadrangles, Alaska: Alaska Division of Geological & Geophysical Surveys Raw Data File 2011-4, v. 2, 176 p. http://doi.org/10.14509/23002

Paces, J.B., and Miller, J.D., 1993, Precise U-Pb ages of Duluth Complex and related mafic intrusions, northeastern Minnesota—Geochronological insights to physical, petrogenic, paleomagnetic, and

tectonomagmatic processes associated with the 1.1 Ga Midcontinent Rift System: Journal of Geophysical Research, v. 98, n. B8, p. 13,997–14,013.

Paton, C., Woodhead, J.D., Hellstrom, J.C., Hergt, J.M., Greig, A., and Maas, R., 2010, Improved laser ablation U-Pb zircon geochronology through robust downhole fractionation correction: Geochemistry, Geophysics, Geosystems, v. 11, n. Q0AA06. https://doi.org/10.1029/2009GC002618

Patton, W.W., Jr, Tailleur, I.L., Brosgè, W.P., and Lanphere, M.A., 1977, Preliminary report on the ophiolites of northern and western Alaska, *in* Coleman, R.G., and Irwin, W. P., eds., North American ophiolites: Oregon Department of Geology and Mineral Industries Bulletin 95, p. 51–57.

Patton, W.W., Jr., Miller, T.P., Chapman, R.M., and Yeend, Warren, 1978, Geologic map of the Melozitna Quadrangle, Alaska: U.S. Geological Survey Miscellaneous Geologic Investigations Map I-1071, scale 1:250,000.

Patton, W.W., Jr., Wilson, F.H., Labay, K.A., and Shew, Nora, 2009, Geologic map of the Yukon-Koyukuk basin, Alaska: U.S. Geological Survey Scientific Investigations Map 2909, 2 sheets, scale 1:500,000.

Puchner, C.C., Smith, G.M., Flanders, R.W., Crowe, D.E., and McIntyre, S.C., 1998, Bedrock geology of the Ruby/Poorman mining district, Alaska: Alaska Division of Geological & Geophysical Surveys Report of Investigation 98-11, 12 p., 3 sheets, scale 1:63,360. http://doi.org/10.14509/2587

Renne, P.R., Swisher, C.C., Deino, A.L., Karner, D.B., Owens, T.L., and DePaolo, D.J., 1998. Intercalibration of standards, absolute ages and uncertainties in $^{40}Ar/39Ar$ dating. Chemical Geology, v. 45, p. 117–152.

Roeske, S.M., Dusel-Bacon, Cynthia, Aleinikoff, J.N., Snee, L.N., Lanphere, M.A., 1995, Metamorphic and structural history of continental crust at a Mesozoic collisional margin, the Ruby terrane, central Alaska: Journal of Metamorphic Geology, v. 13, p. 25–40.

Roeske, S.M., McClelland, W.C., and Bradley, D.C., 2006, Ruby terrane, north-central Alaska: Composite of continental affinity rocks [abs]: Geological Society of America Abstract with Programs, 102nd Annual Meeting of the Cordilleran Section, GSA, 81st Annual Meeting of the Pacific Section, AAPG, and the Western Regional Meeting of the Alaska Section, Society of Petroleum Engineers, Paper no. 8-2.

Steiger, R.H., and Jager, E., 1977, Subcommission on geochronology; Convention on the use of decay constants in geo- and cosmochronology: Earth and Planetary Science Letters, v. 36, p. 359–362.

Thomas, B.I., and Wright, W.S., 1948, Investigation of the Tozimoran Creek tin placer deposits, Fort Gibbon district, Alaska: U.S. Bureau of Mines Report of Investigations 4323, 11 p. https://dggs.alaska.gov/pubs/id/21528

Twelker, Evan, and O'Sullivan, P.B., 2021, U-Pb zircon data and ages for bedrock samples from the Richardson mining district, Big Delta Quadrangle, Alaska: Alaska Division of Geological & Geophysical Surveys Raw Data File 2020-14, 17 p. https://doi.org/10.14509/30555

Vermeesch, Pieter, 2018, IsoplotR: a free and open toolbox for geochronology. Geoscience Frontiers, v.9, p. 1,479–1,493. https://doi.org/10.1016/j.gsf.2018.04.001

Vermeesch, Pieter, 2021, On the treatment of discordant detrital zircon U–Pb data: Geochronology, v. 3, p. 247–257. https://doi.org/10.5194/gchron-3-247-2021

Wildland, A.D., Wypych, Alicja, Regan, S.P., and Holland, Mark, 2021, U-Pb zircon ages from bedrock samples collected in the Tanacross and Nabesna quadrangles, eastern Alaska: Alaska Division of Geological & Geophysical Surveys Preliminary Interpretive Report 2021-4, 47 p. https://doi.org/10.14509/30732

Zhang, M., Ewing, R.C., Boatner, L.A., Salje, E.K.H., Weber, W.J., Daniel, P., Zhang, Y., and Farnan, I., 2009, Pb* irradiation of synthetic zircon ($ZrSiO_4$); Infrared spectroscopic study—Reply: American Mineralogist, v. 94, p. 856–858.